AGU PUBLICATIONS

JGR

Journal of Geophysical Research: Atmospheres

RESEARCH ARTICLE
10.1002/2015JD023130

Key Points:
- Regional characteristics of tropical expansion examined with radiosonde data
- Tropical expansion since 1979 largest over Asia and Australia-New Zealand
- Climate variability significantly affects the observed rate of expansion

Supporting Information:
- Text S1, Figures S1–S3, and Tables S1–S9

Correspondence to:
C. Lucas,
c.lucas@bom.gov.au

Citation:
Lucas, C., and H. Nguyen (2015), Regional characteristics of tropical expansion and the role of climate variability, *J. Geophys. Res. Atmos.*, *120*, doi:10.1002/2015JD023130.

Received 19 JAN 2015
Accepted 9 JUN 2015
Accepted article online 11 JUN 2015

Regional characteristics of tropical expansion and the role of climate variability

Christopher Lucas[1] **and Hanh Nguyen**[1]

[1]Bureau of Meteorology, Melbourne, Victoria, Australia

Abstract Radiosonde-based tropical expansion rate estimates for six continental-centered regions of the globe are discussed. New results from the Northern Hemisphere are presented, complementing previous Southern Hemisphere (SH) results using an identical methodology. Expansion rates are largest over Asia and Australia-New Zealand (ANZ). Other regions show more modest rates of expansion, and there is no statistically significant expansion over North America. In the hemispheric average, expansion rates are slightly larger in the SH. This asymmetry, although not statistically significant, is consistent with ozone depletion acting as a codriver of tropical expansion since 1979. The picture of regional expansion here is different from that in other studies or that derived solely from reanalyses. The relationships between tropical expansion and modes of climate variability are explored using partial regression techniques. Interannually, a relationship is seen with the El Niño–Southern Oscillation (ENSO) across most of the globe. Regionally, the Pacific Decadal Oscillation (PDO) has a significant impact over Asia, while the Southern Annular Mode (SAM) affects expansion over ANZ. Considering the longer-term changes in the climate variability indices since 1979, it suggests that the PDO may account for up to 50% of the observed tropical expansion over Asia, while SAM may account for 20–30% of the SH expansion, particularly over ANZ. Decadal changes in ENSO may account for a further 20–30% of the global and regional trends. Accounting for the effect of climate variability helps to reconcile the differences in observations and model-based simulations of tropical expansion.

1. Introduction

Tropical expansion has been robustly observed around the globe using multiple data sets and methodologies. From the review of *Lucas et al.* [2014], a consensus of the observations suggests that the rate of this expansion since 1979 lies between 0.5 and 1.0° latitude per decade in both the Northern (NH) and Southern (SH) Hemispheres. The precise expansion rates and their hemispheric and longitudinal partitions remain significant unknowns.

Many factors potentially contribute to the uncertainty in these estimates. There are multiple metrics that have been used to define the "tropical edge," and these metrics may respond differently to the forcing driving the expansion because of their differing physics [e.g., *Davis and Rosenlof*, 2012]. Further, many estimates are based on one or more of the global reanalysis products; these model-observation hybrid products may not be suitable for the analysis of climate trends due to changes to the global observing system that may create significant inhomogeneities in the record [e.g., *Bengtsson et al.*, 2004]. One such suspected inhomogeneity affecting tropical expansion calculations was identified in the ERA Interim reanalysis by *Lucas et al.* [2012], hereafter LNT12], likely related to changes to the satellite observing system in the early 2000s.

Uncertainty also arises because the forcing factors driving tropical expansion and the mechanisms by which they work are only partially understood. Climate models, which generally simulate a notably smaller response (0.1–0.2° decade^{-1}) than has been observed [e.g., *Johanson and Fu*, 2009; *Quan et al.*, 2014], have been crucial to our understanding. As summarized in *Lucas et al.* [2014], the tropical expansion trend is largely considered to be a response to anthropogenic climate forcing. Increasing greenhouse gases (GHG) are a likely culprit, either as a direct response to the radiative forcing or as an indirect response from related changes in sea surface temperature (SST) patterns [e.g., *Staten et al.*, 2012; *Quan et al.*, 2014]. This GHG response is expected to be symmetric about the equator [e.g., *Seager et al.*, 2010]. For the NH, anthropogenic "absorbing" aerosol (e.g., black carbon) has been proposed to be a driver behind expansion [*Allen et al.*, 2012a]. In the SH, Antarctic stratospheric ozone depletion is likely a factor [e.g., *Son et al.*, 2009, 2010; *Polvani et al.*, 2011; *Min and Son*, 2013], perhaps resulting in an asymmetric response with greater

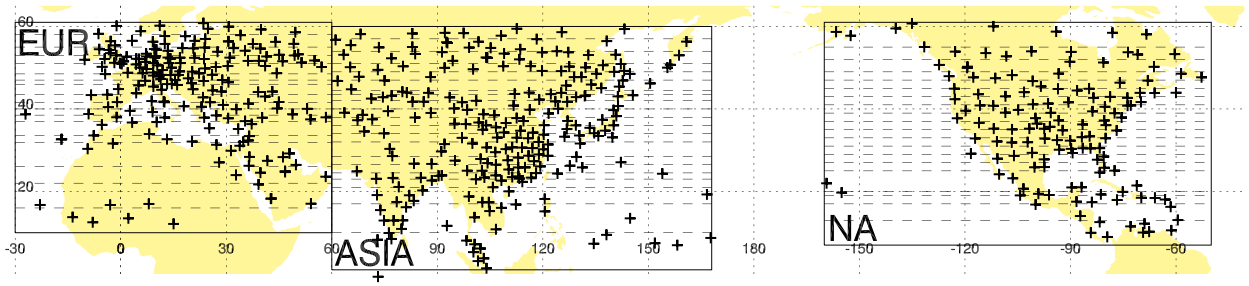

Figure 1. Map of radiosonde sites (crosses) used in this analysis. Large boxes depict the boundaries of regional analysis. Within each region, dashed lines identify the limits of the zonal bands used in constructing the composite time series.

expansion in the SH. The relative amounts that these individual forcings contribute to the total expansion remains unknown.

While modeling studies point to an anthropogenic driver, natural climate variability is also known to influence the position of the tropical edge. For example, the El Niño–Southern Oscillation (ENSO) modulates the tropical edge such that it is wider during the La Niña phase [e.g., *Oort and Yienger*, 1996; *Nguyen et al.*, 2013]. Other modes of climate variability may play a role in tropical expansion as well. The annular modes [e.g., *Thompson and Wallace*, 1998], here called the Arctic Oscillation (AO) in the NH and the Southern Annular Mode (SAM) in the SH, are a major source of variability in the extratropics, and have been linked to circulation anomalies in tropics and subtropics [e.g., *Chen et al.*, 2014a; *Hendon et al.*, 2014]. The Pacific-North America (PNA) pattern [e.g., *Leathers et al.*, 1991] has been linked to significant interannual variability in storm tracks over North America [*Grise et al.*, 2013]. The PNA pattern is also linked to the tropical circulation, where deep convection over the western Pacific stimulates Rossby waves, which subsequently propagate into North America [e.g., *Moore et al.*, 2010]. Over Europe, the North Atlantic Oscillation (NAO) [e.g., *Hurrell et al.*, 2003; *Folland et al.*, 2009] affects circulation and storm tracks on time scales ranging from daily to decadal. At decadal time scales, the Pacific Decadal Oscillation (PDO) [e.g., *Mantua and Hare*, 2002] has also been reported to directly influence tropical expansion [*Grassi et al.*, 2012; *Allen et al.*, 2014]. The Atlantic Multidecadal Oscillation (AMO) [*Schlesinger and Ramankutty*, 1994; *Enfield et al.*, 2001] is known to impact tropical rainfall and Atlantic hurricanes, along with North American and European summer climate [e.g., *Knight et al.*, 2006].

Most work on tropical expansion to date has been focused on zonal-average or global behavior. Only a few recent studies have described its regional variability, which may be important for understanding the local impacts of the expansion. LNT12 used radiosonde-based tropopause measurements over three broad SH continental regions, finding greater expansion over the Australia-New Zealand (ANZ) region. *Choi et al.* [2014] examined the variation of the SH subtropical ridge, indicating that most of the 0.22° decade^{-1} expansion was occurring around Australia and the southern Atlantic Ocean. *Chen et al.* [2014b] investigated variation in the regional Hadley circulation from reanalysis and outgoing longwave radiation (OLR) measurements over six regions. In their analysis, expansion was reported in most regions of the NH, while only South America showed significant expansion in the SH.

In this study, the techniques developed by LNT12 are used to examine tropical expansion in three land-centered regions of the NH (Figure 1). The radiosonde-based findings are compared to reanalysis-derived results to further investigate the fidelity of those products, along with the potential homogeneity issues raised by LNT12. Combining the NH results of this paper with those from the SH in LNT12, we present an observationally based depiction of regional tropical expansion for six broad continental areas around the globe. The expansion is compared between regions as well as across the NH and SH. Finally, the annual tropopause-based metric used here is statistically related to the modes of climate variability noted above in order to examine the role of natural climate variability on tropical expansion trends.

2. Data and Methods

2.1. Regional Tropical Expansion Estimates in the NH

For this study, we follow the protocol of LNT12 for the processing and analysis of the data. This method, described in detail in LNT12, is briefly summarized here.

The radiosonde data used in this study come from the Integrated Global Radiosonde Archive (IGRA) [*Durre et al.*, 2006]. As in LNT12, we adopt the philosophy of including all available stations in our analysis rather than selecting a subset of stations with the most complete records. From these data, the height of the lapse-rate tropopause, Z_T, is independently calculated. Through visual analysis of the resulting time series data, stations with obviously inhomogeneous or spatially inconsistent records are removed. Further, individual observations where Z_T is identified on a "mandatory level" are also removed. This generally results from a lack of "significant level" data within the sounding and most often represents a poor determination of Z_T. LNT12 indicated that extended periods where these data occurred were associated with inhomogeneous time series of Z_T data.

To facilitate the analysis, the NH is divided into three broad regions (Figure 1): North America (NA), Europe, including northern Africa and the Middle East (EUR) and Asia (ASIA). The boundary between ASIA and EUR is subjectively drawn at 60°E. The longitudinal distribution of stations (Figure 1) shows a minimum here, making this a natural dividing point. We verified that the overall results are not sensitive to small differences in the choice of longitude for the boundary. Each region extends from 10°N (or further south) to poleward of 60°N; further stations were available poleward of the northern limit, but there is little to be gained in this study from their inclusion. The quantity of stations in this study (Figure 1) are far more numerous than in LNT12, with 136, 178, and 252 stations for NA, EUR, and ASIA, respectively. Figures S1–S3 and Text S1 in the supporting information provide a closer examination of the data availability by station and by year. The aim is to extend the calculation as far back as possible. Hence, the start time in each region is different, based on the quality of the available data. Start times are 1965, 1979, and 1970 for NA, EUR, and ASIA, respectively; the common period covered begins in 1979.

Within each region, we construct a "time-latitude" array to estimate the rate of tropical expansion, adapting the Tropopause Height Frequency technique described by *Seidel and Randel* [2007]. The Z_T data are analyzed to determine the annually normalized number of tropical tropopause days (TTD), defined as days where the Z_T lies above a fixed threshold of 14.5 km. This raw annual TTD value is adjusted to account for the sampling bias introduced by missing or unevenly timed data. For this study, the "year" over which the data are analyzed runs from December to the following November, shifted by 6 months from the June to May period used in LNT12. These timings place the start date of each year at the beginning of winter in the respective hemisphere, keeping the evolution of the annual cycle of Z_T for a given year coherent within the TTD metric.

Spatially, the data are organized into latitude bands, generally 2–3° latitude in width. These bands, delineated by horizontal dashed lines in Figure 1, are nonuniform and are subjectively determined to maximize the data availability and to minimize the horizontal resolution. In NA, EUR, and ASIA, 20, 19, and 21 bands are used, respectively. Figures S1–S3 provide greater detail regarding the limits and station composition of these bands. For each band, a composite time series is created using a "first difference" approach analogous to that of *Peterson et al.* [1998], a technique that is relatively resistant to inhomogeneities in the data [*Peterson and Easterling*, 1994]; LNT12 provide a detailed discussion and examples of these procedures. The time-latitude array that results from this process is contoured at TTD = 300, 200, 100, and 50 days, and the slope (i.e., the change in latitude with time) of these individual contours provides the tropical expansion estimates.

Despite the greater amount of data compared to LNT12, the tropopause sampling in some portions of the NH regions has gaps in its coverage. One region of particular concern is the Mediterranean portion of EUR, where most of the stations in the relevant bands are located in the Middle East; there is a lack of stations across much of the Sahara and northern Africa. A second region of concern is found between 20 and 25° in the NA region, where relatively few stations are available. LNT12 noted similar concerns for the SH, particularly in regards to data quality in Africa and some portions of South America. In ASIA, the amount of data available dramatically increases after 1990, when data from the radiosonde network over China are added to the IGRA archive.

There are potential concerns about the analysis methodology. As with any extended climate record, significant inhomogeneities in Z_T from the radiosonde data could impact estimates of the rate of expansion. The more egregious inhomogeneities within the data have been manually removed, as noted earlier; other more subtle examples undoubtedly remain. Following the discussion of LNT12, the simple

Table 1. Modes of Climate Variability Examined in This Study and the Source of the Index Data Describing Each Mode

Mode	Data Obtained From
ENSO	Mulitvariate ENSO Index (MEI) :http://www.esrl.noaa.gov/psd/enso/meil *Wolter and Timlin* [1998]
PNA, AO, NAO	NOAA Climate Prediction Center (http://www.cpc.ncep.noaa.gov/products/precip/CWlink/daily_ao_index/teleconnections.shtml)
PDO	Japanese Meteorological Agency Tokyo Climate Center (http://ds.data.jma.go.jp/tcc/tcc/index.html)
AMO	http://www.esrl.noaa.gov/psd/data/timeseries/AMO/ *Enfield et al.* [2001]
SAM	http://www.nerc-bas.ac.uk/icd/gjma/sam.html *Marshall* [2003]

TTD metric is insensitive to small jumps in the data if they do not cross the defined Z_T threshold. Further, the compositing technique is generally resistant to data artefacts as noted earlier.

Other critiques are centered on the choice of the Z_T threshold. *Birner* [2010] suggests that the results are highly sensitive to the chosen value of the fixed height threshold. *Davis and Rosenlof* [2012] speculate that a fixed threshold creates a "sympathetic trend" associated with the "background" rise in global Z_T, overestimating the "true" expansion rate. LNT12 examined these issues and found little sensitivity to threshold choice in the results within the SH observational data; uncertainties were more related to the characteristics of the data rather than the technique itself. LNT12 also suggested that "trend removal" techniques were highly reanalysis dependent and not physically robust. Estimates of the sympathetic trend by LNT12 suggested that it accounted for less than 20% of the observed trend. Based on these findings, we believe that these methodology-related issues have little impact and do not make a significant difference to the final results.

2.2. Effects of Modes of Climate Variability

The relationships between tropical expansion, as estimated from the TTD contours, and the modes of climate variability described in the Introduction are explored using partial correlation and partial regression analyses. With these analyses, the influence that modes of climate variability have on the positions of the individual TTD contours is identified. Correlation identifies whether a relationship exists, while regression indicates the magnitude of the effect. To remove spurious correlations caused by coincident trends in the separate variables, all variables are linearly detrended before analysis, leaving only the interannual relationships.

The instantaneous state of each of these seven modes of climate variability is represented by a monthly index. Time series of the index describing each mode are obtained from the sources indicated in Table 1. The monthly time series are annually averaged over the appropriate year for each hemisphere (section 2.1) to match the timing of the TTD contours. "Partial" techniques are used as many of the modes are not independent; these methods are designed to isolate the effect of a given variable by linearly removing the effects of each of the other "control" variables from both the dependent and independent data [e.g., *Panofsky and Brier*, 1968]. Standard correlation/regression techniques are performed on the resulting residuals, yielding the partial coefficients. Statistical significance is assessed using a standard t test, with the degrees of freedom equal to $N\text{-}M-2$, where N is the number of years and M is the number of control variables removed, six in all cases here. Statistical significance is generally assumed at 95%, although in several instances correlations with 90% significance are noted where warranted. Table S1 details the various significance thresholds in the different regions; these are variable because of the different numbers of years in each time series.

The statistical analysis is performed in several ways. First, annually averaged climate mode indices are related to the hemispheric-average TTD contours (termed "global" contours), yielding a hemispheric view that is compatible to earlier studies. Second, annual TTD contours from each individual region are related to the annually averaged climate indices, providing information on what factors are important on a regional basis. Finally, seasonally averaged climate indices are related to the annual TTD contour positions, identifying the particular season when a mode of variability influences the annual number of TTDs. Seasonal averages are calculated over the standard meteorological seasons (i.e., December-January-February (DJF), March-April-May (MAM), June-July-August (JJA), and September-October-November (SON)) from the monthly climate index data.

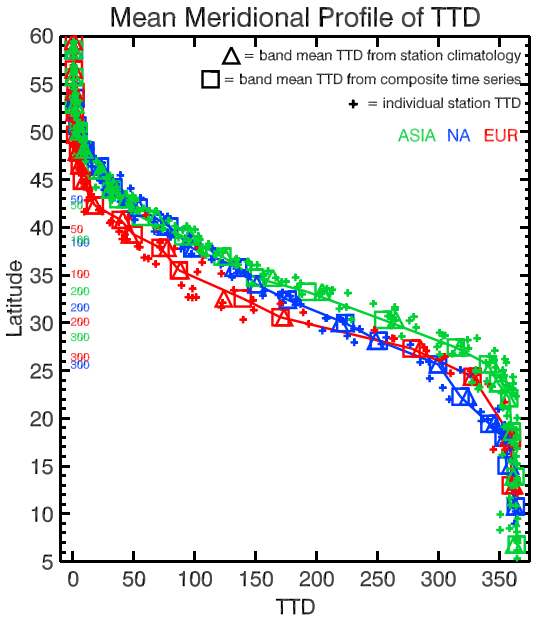

Figure 2. Regional mean TTD profiles. ASIA = green, NA = blue, EUR = red. The squares show mean based on mean of band composite time series. The triangles show mean of climatological TTD for all stations in band. The small symbols indicate climatological TTD for individual stations. Mean position of standard contours for each region denoted by numbers on left.

3. Tropical Expansion in the NH

3.1. Mean Structure and Variability of NH TTD

Figure 2 shows the mean structure of TTD of each region, highlighting their broad meridional characteristics. Across the NH the subtropics, loosely defined following LNT12 as the region between the 300 and 50 day contours, generally extends between 26°N and 43°N. Equatorward of this area lie the tropics; the extratropics are found poleward of this region. Despite the broad similarity, meaningful regional differences are seen in the position of the subtropics. In ASIA, the 300 and 200 day contours are found 2–4° farther north than other regions. In EUR, most contours are found at lower latitudes than the other regions; this is particularly noticeable toward the extratropics, where the 50 and 100 day contours are 2–4° farther south than the other regions. The NA region resembles EUR at lower latitudes but is more similar to ASIA at higher latitudes.

Figure 2 also shows meridional profiles of band-averaged TTD derived from the mean value of the composite time series and that derived from mean climatological TTD value (TTD_C) of the stations comprising the band. The RMS differences between the profiles range from 2 to 6 days, giving confidence that no large "random walk" errors [*Free et al.*, 2004] have been introduced by the first difference technique used to construct the composite time series. The EUR6 band has a large difference (~15 days) due to missing data affecting the initial value of the series; bands ASIA8-10, 13 have differences greater than 10 days because of the sudden inclusion of data from China in 1991. The TTD_C of these Chinese data are likely biased high because they do not sample the earlier part of the record when TTD is lower. In these cases, visual inspection of the time series confirms that there is no significant random walk error.

Figure 3 presents the TTD contours for each of the analyzed NH regions. Individual contours are referred to in "shorthand" by the region and the TTD value (e.g., ASIA300). The different regional mean structures noted in

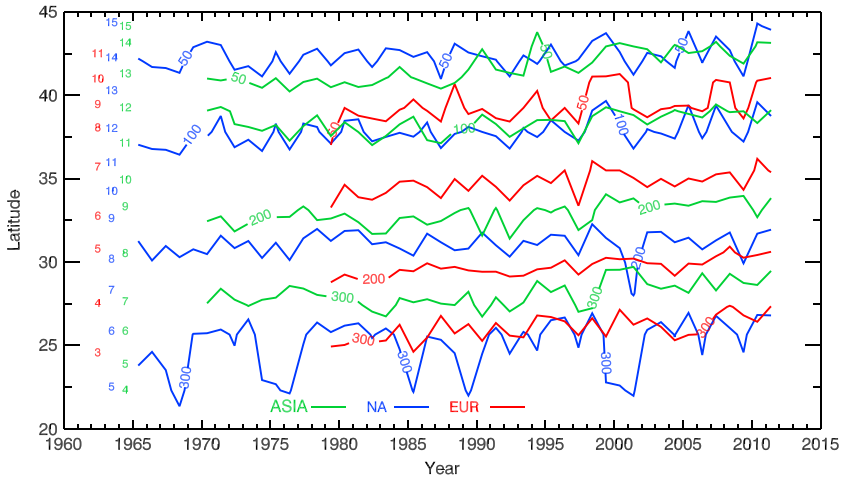

Figure 3. Regional comparison of TTD contours. Small numbers on left represent the location of the bands in each region.

Table 2. Linear Trends With 2-Sigma Confidence Intervals for Radiosonde-Observed TTD Contours[a]

Region	300	200	100	50
NH				
NA	0.22 ± 0.67	−0.02 ± 0.33	0.28 ± 0.33	0.24 ± 0.37
EUR	**0.47 ± 0.23**	**0.43 ± 0.17**	**0.41 ± 0.30**	**0.54 ± 0.35**
ASIA	**0.59 ± 0.27**	**0.49 ± 0.23**	**0.47 ± 0.20**	**0.79 ± 0.24**
NH global	**0.42 ± 0.20**	**0.29 ± 0.15**	**0.38 ± 0.20**	**0.52 ± 0.22**
NA (1965–2011)	0.31 ± 0.42	0.08 ± 0.18	**0.28 ± 0.19**	0.18 ± 0.19
ASIA (1970–2011)	**0.34 ± 0.24**	**0.33 ± 0.15**	**0.22 ± 0.21**	**0.64 ± 0.17**
SH				
ANZ	**−0.34 ± 0.20**	**−0.74 ± 0.34**	**−0.58 ± 0.39**	−0.26 ± 0.52
SA	**−0.94 ± 0.58***	**−0.45 ± 0.21**	**−0.94 ± 0.38***	**−1.23 ± 0.60***
AFR	+0.05 ± 0.37*	−0.26 ± 0.34	**−0.34 ± 0.29**	**−0.22 ± 0.16**
SH global	**−0.32 ± 0.29**	**−0.45 ± 0.23**	**−0.57 ± 0.26**	**−0.49 ± 0.38**

[a]Trends are estimated over 1979–2011 except where indicated. SH values taken from LNT12. The sign of expansion is positive in NH and negative in SH. Trends significant at the 95% level, accounting for autocorrelation effects, are in bold. Asterisks indicates the less reliable contours noted in the text. Units are deg decade^{-1}.

Figure 2 are readily discerned from the position of the contours. Long-term expansionary trends are apparent throughout the NH. However, both the expansion rate and the interannual variability differ in each region.

In general, trends from 1979 to 2011 (Table 2) range from near zero (NA200) to almost 0.8° decade^{-1} (ASIA50). Only in ASIA and EUR do the trends exceed the 2σ confidence intervals; in NA the trends are not statistically significant. Averaging the regional contour positions (using weights based on the relative defined area of each region) suggests that the global NH trend lies between 0.3 and 0.5° decade^{-1}. Considered from 1970, trends in ASIA are smaller, often less than half their value compared to the shorter period, but remain statistically significant. In NA, trends since 1965 are generally in the same range compared to the values since 1979, and with one exception (NA200) remain statistically insignificant.

Figure 3 also shows that the interannual variability is different between the regions, most notably on NA300 where the contour shows strong "dips" where the contour shifts equatorward by 2–3° latitude for 1 to 3 years. Examples are seen in 1968, 1973–1976, 1985, 1989, and 1999–2001. The meteorological phenomenon behind these dips is not known. Perusal of the composite time series and their component stations (not shown) for the relevant bands shows broad agreement across numerous stations; this is a robust phenomenon and is not driven by faulty observations at a few stations.

3.2. Reanalysis Comparison

As in LNT12, we compare the radiosonde-based results with those derived from four reanalysis products—the NCEP (National Centers for Environmental Prediction)/NCAR reanalysis (NCEP [*Kalnay et al.*, 1996]), the NCEP/DOE (Department of Energy) reanalysis (NCEP2 [*Kanamitsu et al.*, 2002]), the ERA 40 year reanalysis (ERA-40 [*Uppala et al.*, 2005]) and the ERA Interim (ERA-I [*Dee et al.*, 2011]). The reanalyses are selected on the basis of the availability (to us) of daily fields for the required computations. We use these data from 1980 to 2010 with the algorithm defined in *Reichler et al.* [2003] to determine Z_T and the number of TTD over the same regions and bands defined in Figure 1. This is done by direct estimation of these quantities rather than through the sampling methods used with the observations.

Overall, the results of the radiosonde/reanalysis comparison (Figure 4) are similar to what was identified in LNT12. On an interannual basis the match is quite good, with high correlations (0.8–0.9) between detrended observed and reanalysis-derived TTD contours, with lower values (0.5–0.7) found in some of the data-sparse regions noted earlier. The dips noted on NA300 are captured in the reanalysis, although not as strongly as in the observations, supporting our interpretation of these as real phenomena. While interannual variability matches well, the positions of the reanalysis contours are generally shifted poleward of their observed position, particularly in the "tropical" portion of the subtropics (i.e., 200 and 300 day contours). This "shift" is typically about 1–3° latitude and as discussed in LNT12, it is believed to arise from shortcomings in the tropopause algorithm and the relatively coarse vertical resolution of the reanalysis data.

Trends in the reanalysis-based TTD contours are mixed, with fewer instances of expansionary trends identified (Table 3). In NA, the tropical contours in the ERA-40 and ERA-I indicate contractive trends, strongly so on the

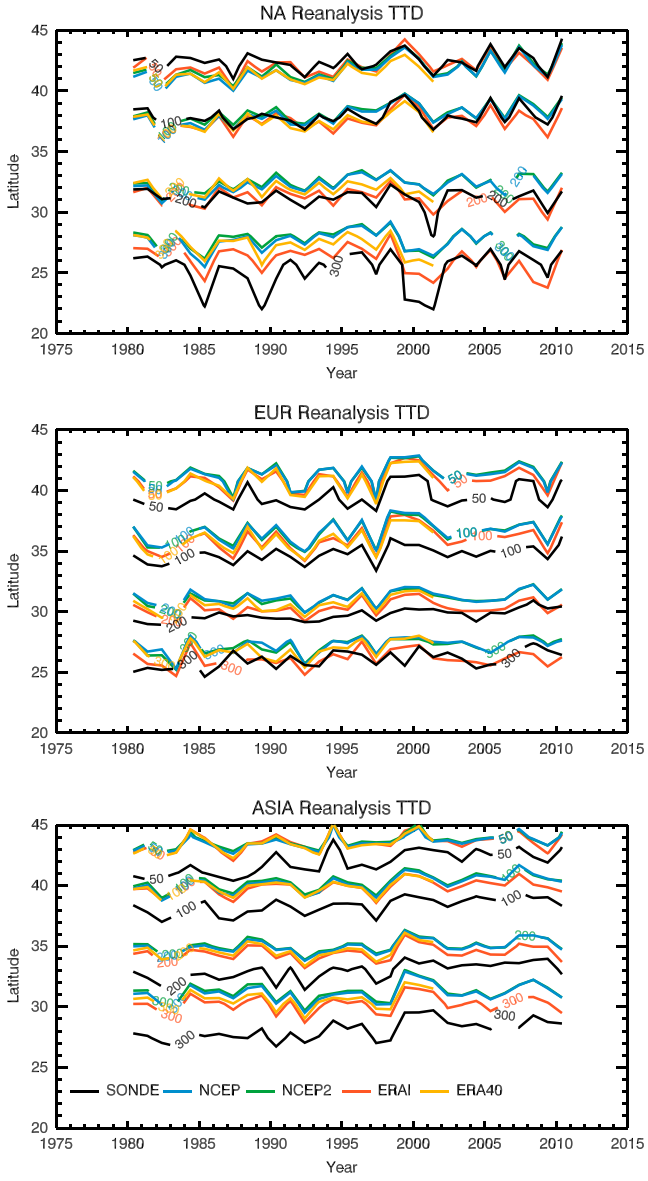

Figure 4. Comparison of radiosonde and reanalysis derived TTD contours for the (top) NA, (middle) EUR, and (bottom) ASIA regions for the 1980–2010. Sonde contour positions are same as those in Figure 3.

300 day contours; these are only statistically significant in the ERA-I. In EUR, expansion trends are, in general, slightly smaller than those observed in the radiosondes. Similarly in ASIA, the trends are generally smaller than those in the observational data.

The spatial and temporal characteristics of the shift noted above are crucial to understanding the differences in trend between radiosonde and reanalyses. The shift varies by region. Overall, the shift is smallest in EUR and largest in ASIA. In NA, the 200 day and "extratropical" (i.e., 100 and 50 day) contours show the best fit and the shift is very small on average. Earlier in the analysis period, an equatorward shift is observed here. However, NA300 is an exception, showing a large shift and a significant variability in time. The very good fits of the NA100 and NA50 occur in the heart of the U.S. sonde network, the best sampled, most consistent set available (see Figures S1–S3). We speculate that the strong match here likely represents the strong influence of the "terrestrial" observing system on constraining the reanalyses in this region [*Bengtsson et al.*, 2004]. In general, the older "first generation" reanalysis products (NCEP, NCEP2, and ERA-40) have a larger shift, while the newer ERA-I has a variable performance. Prior to 2002, the ERA-I shift is comparable to the other products; in the latter period, the ERA-I shows much better agreement with the observations. This improvement is particularly noticeable on NA300. All contours in ASIA show a smaller shift in the last 8 years of the record, while in EUR the shift shows little change with time.

Figure 5 summarizes the reanalysis-radiosonde comparisons, showing the behavior of the NH200 and NH50 contours. In the figure, the mean position of each contour is removed (eliminating the shift), allowing for a direct comparison of the behavior of the contours from different sources. For NH200 (top), there is good agreement—with some comparatively minor differences (e.g., late 1980s)—between the radiosonde and reanalysis-derived positions until the year 2001. From 2001 to 2007, the reanalyses consistently suggest behavior that differs from the radiosonde data. After 2007, the NCEP and NCEP2 begin to match the sonde data again, while the ERA-I remains separate. The behavior of the NH300 (not shown) is similar to NH200. Similar behavior of the 200 day contour in the ERA-I was noted by LNT12 and speculatively attributed to changes in the global satellite observing system that occurred. For NH50 (bottom), the agreement between reanalysis and radiosonde-derived global contours is excellent, with only a few minor deviations between the various sources. NH100 (not shown) behaves similarly to NH50. This suggests that

Table 3. NH Regional Trends and 2-Sigma Confidence Intervals for Reanalysis-Based TTD Contours[a]

NA	NCEP	NCEP2	ERA-I	ERA 40	Radiosonde
300	0.01 ± 0.35	0.14 ± 0.37	**−0.47 ± 0.43**	−0.44 ± 0.61	0.22 ± 0.67
200	0.23 ± 0.30	**0.32 ± 0.28**	−0.18 ± 0.41	−0.14 ± 0.64	−0.02 ± 0.33
100	**0.49 ± 0.35**	**0.59 ± 0.34**	0.23 ± 0.39	0.28 ± 0.55	0.28 ± 0.33
50	**0.57 ± 0.39**	**0.66 ± 0.39**	0.34 ± 0.41	0.33 ± 0.53	0.24 ± 0.37
EUR					
300	**0.33 ± 0.30**	0.28 ± 0.33	0.16 ± 0.29	0.51 ± 0.56	**0.47 ± 0.23**
200	**0.30 ± 0.24**	**0.26 ± 0.25**	0.23 ± 0.25	**0.50 ± 0.44**	**0.43 ± 0.17**
100	0.38 ± 0.41	0.37 ± 0.42	**0.42 ± 0.39**	**0.74 ± 0.72**	**0.41 ± 0.30**
50	0.29 ± 0.47	0.31 ± 0.47	0.33 ± 0.41	0.55 ± 0.82	**0.54 ± 0.35**
ASIA					
300	0.15 ± 0.35	0.22 ± 0.36	0.11 ± 0.30	0.27 ± 0.54	**0.59 ± 0.27**
200	0.19 ± 0.28	0.24 ± 0.28	0.15 ± 0.28	0.25 ± 0.55	**0.49 ± 0.23**
100	**0.36 ± 0.27**	**0.44 ± 0.29**	0.23 ± 0.28	0.31 ± 0.49	**0.47 ± 0.20**
50	**0.31 ± 0.26**	**0.34 ± 0.24**	**0.28 ± 0.28**	0.50 ± 0.53	**0.79 ± 0.24**

[a]Trends computed over period from 1980 to 2010 (2001 for ERA-40). Expansion represented by a positive trend; trends that are significant at 95% level, accounting for autocorrelation effects, are in bold. Radiosonde-based values from Table 2 are shown for comparison. Units are deg decade^{-1}.

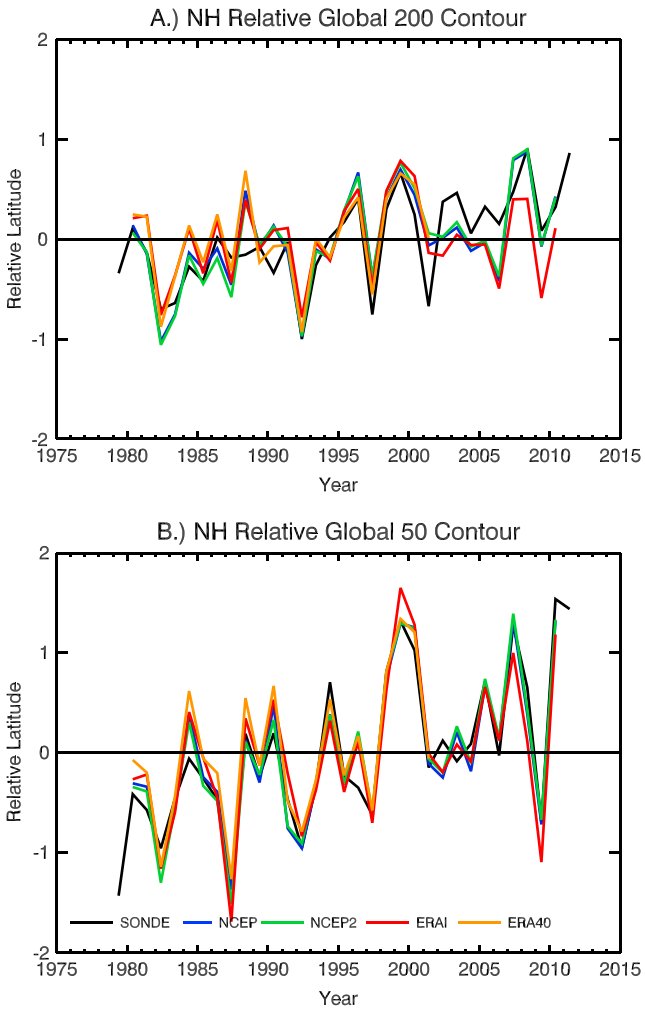

Figure 5. The relative global (a) 200 day and (b) 50 day TTD contours from radiosonde and the four reanalyses examined. The zero line represents the mean value of the contour in each analysis.

any inhomogeneity within reanalysis products from this source is limited in scope to equatorward of ~35° latitude.

4. Global Complexities of Tropical Expansion

The above results for NH tropical expansion are combined with those for the SH from LNT12 to present an observationally based picture of tropical expansion across six broad continental regions around the globe (see Figure 7 for SH regions). While the methodology between the two studies is identical, the lack of consistent reliable data in parts of the SH limits the confidence in some of the calculated TTD contours. The 200 day TTD contours are reliable in all regions of the SH, and the most confidence placed (on all contours) from the ANZ region due to better data quality there. LNT12 found that compared to reanalysis data, interannual variability was adequately captured even on less reliable contours, but significant uncertainty remains in the estimate of the long-term trends (Table 2).

4.1. Tropical Expansion in the NH and SH

Figure 6 shows the time-latitude position of the average (i.e., global) NH and SH (sign reversed) contours. Significant

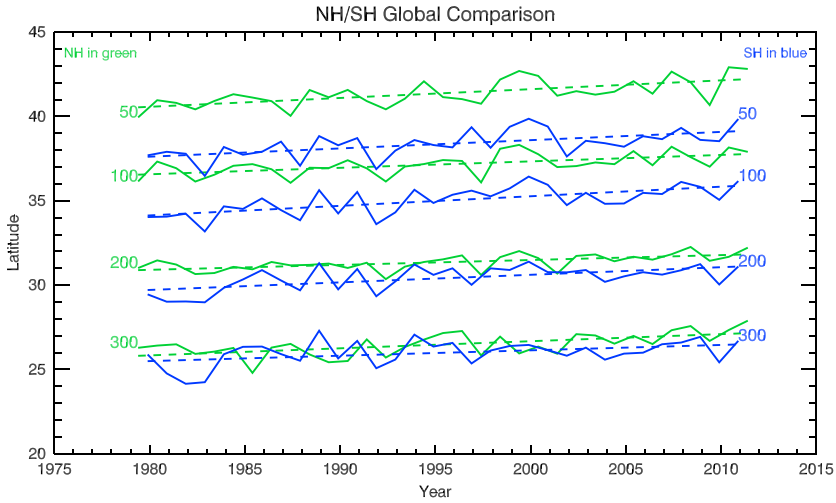

Figure 6. Comparison of NH (green) and SH (blue) global contours. Sign has been reversed on SH contours.

differences are observed in the extent of the subtropics, particularly in the extratropical portion (100 and 50 day contours). Here the NH contours are 3–5° latitude more poleward than their relative position in the SH; in the tropical portion (300 and 200 day contours), the distance is 1–2° latitude poleward. Regional variability is also greater in the NH (Figure 2); in the SH, the positions of the contours were more consistent between the regions (see Figure 8 in LNT12).

Rates of expansion (dashed lines in Figure 6; Table 2) are notionally larger in the SH. The 200 and 100 day contours show 50–60% faster expansion in the SH, while the 300 day contour shows ~30% greater expansion in the NH. Differences on the 50 day contour are relatively small ($<$10 %). Following the approach of *Lanzante* [2005] for overlapping confidence intervals, the differences in trends between hemispheres are not significant; the 200 and 100 day contour trend differences between hemispheres represent a difference of just over 1 standard error. Despite the nonsignificance of this result, the slightly greater expansion in the SH is consistent with ozone depletion playing a role in forcing SH tropical expansion. Close examination of Figure 6 shows that the SH tropical contours undergo rapid expansion in the early and mid-1980s, the period when the now-typical springtime Antarctic ozone depletion was being established and becoming a significant climate forcing. Expansion appears to have slowed since the early 2000s [e.g., *Ao and Hajj*, 2013]. However, the fact that the NH shows any expansion at all suggests that ozone depletion—not expected to be a factor in the NH—cannot be the *sole* reason behind tropical expansion, as discussed in *Lucas et al.* [2014]. More investigation is required to quantify the relative effect ozone depletion has in producing SH tropical expansion.

Another difference between hemispheres is the strength of the response to the two major volcanic eruptions during the analyzed period. In the SH, LNT12 noted a 1–2° latitude contraction of the tropics after the eruptions of El Chichón (1982) and Mount Pinatubo (1991), a result of the stratospheric injection of aerosol that depresses tropopause height [e.g., *Santer et al.*, 2003]. A contraction can be detected in the NH (Figure 6), but the signal is not as strong as that identified in the SH; the NH global composite suggests a magnitude of 0.5–1.0° latitude. This asymmetry may appear unusual given that both eruptions occurred well inside (~15–18° N) the NH, but these results are qualitatively consistent with the results of *Free and Angell* [2002] and *Free and Lanzante* [2009]. Those studies note that the zonal-mean stratospheric heating and tropospheric cooling were asymmetrical about the equator, with the strong response limited to regions equatorward of 30°N in the NH, but extended to 40°S and beyond in the SH. The warming was also observed at a lower altitude in the SH. These conditions persisted for 1–2 years after the initial eruptions.

The generality of this observation is unclear. Is the apparent greater contraction in the SH due to volcanic activity a fundamental dynamic response or is this simply a matter of timing of the eruptions? Both eruptions occurred in boreal spring or early summer, a time when the mean meridional circulation at higher altitudes favors flow into the SH. An eruption during boreal winter could see a different result.

Table 4. Linear Trends and 2-sigma Confidence Intervals for the Seven Climate Variability Indices[a]

Time Period	AO	NAO	PNA	MEI	PDO	AMO	SAM
1958–2012	*0.07 ± 0.08*	0.01 ± 0.07	0.04 ± 0.06	0.05 ± 0.16	−0.01 ± 0.26	0.05 ± 0.07	**0.21 ± 0.12**
1968–2012	0.05 ± 0.13	−0.03 ± 0.10	0.07 ± 0.09	0.04 ± 0.24	−0.05 ± 0.38	**0.12 ± 0.04**	**0.27 ± 0.17**
1979–2012	0.01 ± 0.21	*−0.14 ± 0.14*	0.03 ± 0.17	*−0.25 ± 0.27*	**−0.47 ± 0.32**	**0.14 ± 0.06**	*0.24 ± 0.26*
1989–2012	**−0.30 ± 0.28**	**−0.38 ± 0.24**	0.17 ± 0.28	−0.37 ± 0.45	−0.54 ± 0.68	**0.17 ± 0.09**	0.19 ± 0.40

[a]Units for trends are (index units per decade). Trends significant at 95% (90%) confidence in bold (italics). For simplicity, all reported trends here are from annual time series using the NH year (i.e., December–November). Units are deg decade^{-1}.

4.2. Interannual Climate Variability

This section examines the relationships between the climate variability indices (Table 4) and the TTD contours using the partial correlation and partial regression methodology. For clarity and conciseness, the significant results from these analyses are summarized in Figure 7. Appendix A provides a list of acronyms for quick reference. The complete tables of results are provided in Tables S2–S9). The summary is organized by mode of climate variability, briefly describing the significant regional, seasonal, and spatial relationships of each index with the contours. Tropical (TR) and extratropical (ET) contours refer to the set of TTD = [200, 300] day contours and the TTD = [50, 100] day contours, respectively. Regression coefficient magnitude is reported in degrees change of TTD contour per unit of the relevant climate variability index, noted as deg/unit.

Globally, ENSO is the mode of climate variability that has the most widespread impact on the TTD contours, with 7 of 8 global contours showing this relationship, NH300 being the exception. In all regions except AFR, ENSO affects the ET contours, particularly during JJA and SON, resulting in an expansion during La Niña and contraction during El Niño, consistent with *Oort and Yienger* [1996]. The regression coefficient is typically around 0.4–0.5°/unit, although often larger in the SH. Over ASIA and ANZ in particular, ENSO also impacts the TR contours, centered on DJF, with a magnitude of 0.2–0.4°/unit. A closer relationship of the ET contours to ENSO was noted by LNT12. ENSO also impacts the NA300 but has a "reverse" effect in that the

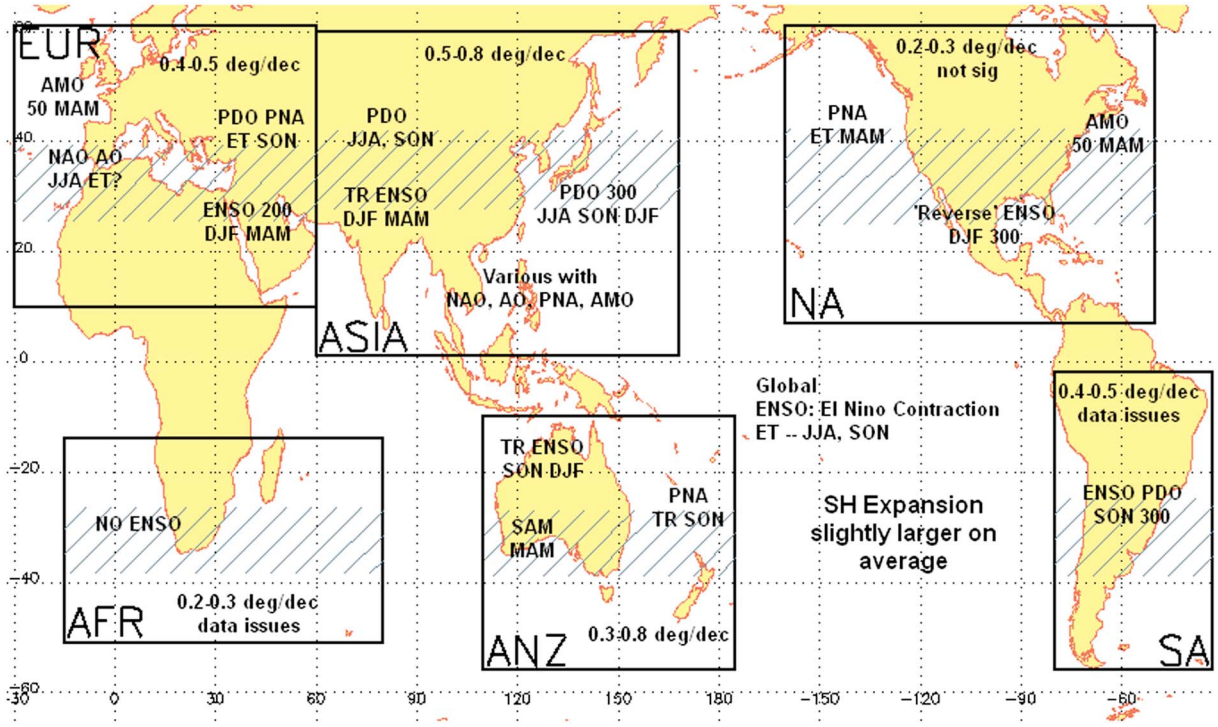

Figure 7. Summary of regional characteristics of tropical expansion. The hatching indicates the mean position of the subtropics identified in each region. Ranges for tropical expansion rates are summarized for each region. Also noted are significant relationships with various modes of climate variability and the contours on which they are identified, noted by either their value, ET (100 and 50 contours), TR (300 and 200 contours), or ALL. The season(s) in which a correlation occurs is also noted. Refer to text for complete description of results.

contour expands during El Niño and contracts during La Niña. This appears to be associated with the dips in that contour noted earlier. This effect is responsible for the lack on ENSO correlation with NH300.

The PDO shows significant correlations with TTD primarily in the NH. This effect is most prevalent over ASIA, occurring in all seasons but MAM and on most contours. A correlation is also noted in EUR during SON; no significant relationships are noted in NA. When the central Pacific is warm (i.e., a negative PDO), the tropics are found further poleward, as in *Allen et al.* [2014]. There is also a significant effect of PDO observed in SA and at the 90% significance level in ANZ. At these SH locations, the effects are on the 300 day contour and act in opposite sense to the NH; the contour is further equatorward during a negative PDO. The typical magnitude of the effect is 0.3–0.5°/unit; the signs of the correlations indicate that the PDO shifts the entire tropical zone toward the North Pole in its negative phase.

The SAM shows weak evidence of an impact on SH100 and SH200, significant at only the 90% level. A highly significant (>99%) correlation with all contours is observed over the ANZ region during MAM. In all cases, a positive SAM results in greater poleward position of all contours, with the size of the effect of 0.3–0.5°/unit. There are also hints of an effect in the NH, with the EUR300 showing significance during DJF. Also during DJF, NA300 and the NH TR contours show a correlation at the lower 90% level. The regressions suggest a weak expansion in the NH during positive SAM.

The PNA primarily affects the NA ET contours during MAM. The correlation is positive, so expansion over NA is expected during the positive phase, which coincides with greater geopotential height anomalies over the USA/Canada border regions (see the loading maps on referenced website in Table 1). A positive correlation is also identified with ANZ TR contours during SON, suggesting a contraction of the tropics in that region. However, rather than a case of "cause and effect" between the PNA and ANZ tropical expansion, the relationship may instead reflect the close relationship between the PNA pattern and convection over the tropical western Pacific through the Madden-Julian Oscillation (MJO) [e.g., *Zhang*, 2005]. Expansion over ANZ may also be linked to the MJO, and this linkage could project onto the PNA index creating the correlation. More investigation is needed to test these hypotheses.

The remaining patterns of climate variability only show weak or inconsistent relationships with the TTD contours. During MAM, the AMO has significant correlations with EUR50 and NA50. Significant relationships are also noted with ASIA100 during SON. The regression coefficients are large here, typically on the order of 1.5–3.0°/unit. However, the AMO index is typically considerably smaller than 1 and changes very slowly.

Most confusing are the results with the NAO and AO time series. These two time series are highly correlated (~0.8 at annual time scales). When significant correlations are found, this pair of variables are often found to offset one another, acting in nearly equal and opposite senses. It is suspected that this is an artefact of the partial correlation technique applied here and the results are not real. The most physically plausible significant correlations identified with these two indices occurs with the EUR ET contours during JJA. More research is required to understand any linkage of observed tropical expansion with these modes of variability.

4.3. Modes of Climate Variability and Observed Tropical Expansion

The previous section demonstrates a linkage between climate variability indices and the position of the various TTD contours on an *interannual* basis. In this section, the effect on tropical expansion is inferred from the correlations/regressions and the longer-term trends in the climate variability indices. The amount of change in a given index, estimated from computed trend, is multiplied by the appropriate partial regression coefficient to yield the amount of change of a given TTD contour that is congruent with the change in the index. From this value, an estimate of the fractional observed change due to a given climate variability index is made. As there are multiple trend estimates and coefficients, these calculations are done over a range reflecting the variability of those estimates.

The interpretation of climate trends, particularly in data series with short records, is difficult [e.g., *Wunsch*, 1999]. Some phenomena, including most of those examined here, exhibit variability occurring over decadal time scales, making the choice of start and end times of the trend calculation a particular concern. Table 4 illustrates this for the climate variability indices used here; the values and statistical significance of the trends often vary considerably depending on the period examined. In some cases (e.g., PDO and ENSO), trends over shorter periods likely reflect changes of phase of a decadal oscillations rather than a longer-term shift. In other cases (e.g., NAO and SAM), the interpretation of the trend over different

intervals is not as clear, but the effects of stochastic variability in the time series cannot be ruled out. Most relevant to this work are the trends over the 1979–2012 period that coincides with the analysis of tropical expansion. The discussion will focus on the trends in PDO, ENSO, SAM, and AMO, as these indices have a trend over the period of interest and show a significant regression in the interannual data.

From 1979 to 2012, the trends in the PDO are significantly negative, associated with a transition from the "warm" (a cooler subtropical western Pacific Ocean) to "cool" phase of the oscillation (Table 4). Over longer periods, trends in the PDO are neutral. The regressed amount of change in the index is estimated at -1 to -1.5 units from 1979, and the TTD regression coefficients is between 0.2 and 0.6°/unit, indicating that the PDO may be responsible for 0.2 to 0.9° latitude of the observed change of the TTD contours. This is particularly relevant over ASIA, where the impact is most pronounced. In terms of the average trend, this is equivalent to 0.05 to 0.27°decade^{-1}, potentially explaining up to 50% of the observed trend over ASIA since 1979. Over the extended record available for ASIA (from 1970; Table 2) trends are 20–50% smaller while the PDO trend is near zero (Table 4); to the degree that this difference is solely due to the climate mode, it provides a comparable estimate of the PDO effect. The magnitude determined here reasonably agrees with the results of *Allen et al.* [2014], who also suggested the PDO accounted for much of trend in the NH but little in the SH.

Closely related to the PDO trend is the trend in ENSO. These two indices are strongly correlated ($r > 0.6$), with the El Niño phase of ENSO observed more frequently when PDO is positive [*Verdon and Franks*, 2006]. The ENSO trend is statistically significant at the 90% level over the 1979–2012 period and indicates a mean index change of -0.5 to -1 units. Given typical regression coefficients (Tables S2–S9), this translates to an total expansion of 0.1 to 0.4° on the TR contours (except in NA) and 0.3 to 0.9° change on the ET contours, with the SH showing expansion in the upper portion of this range. In terms of average trend over the period, this is up to 0.1 and 0.1–0.3° decade^{-1} on TR and ET contours, respectively, potentially amounting to 20–30% of the total observed trend.

SAM is the only pattern examined here that shows statistically significant trends over the longest periods (Table 4). From both 1958 and 1968, significant trends are seen in the annual time series. The trend magnitude from 1979 is about the same as the earlier periods, but the shorter series has increased the size of the confidence intervals and reduced the significance to 90%. Since 1979, these trends have increased the SAM index by 0.8–1.3 units. From the magnitude of the regression, a total change in latitude of the TTD contours of 0.2–0.6° is estimated from 1979, centered over the ANZ region. This is equivalent to an average trend of 0.1–0.2° decade^{-1}, approximately 20–30% of the total trend.

For periods since 1968, the AMO index shows increasing trends (Table 4). From 1979, these trends have increased the index by 0.3–0.5 units. While the change in index in comparatively small, the regression coefficients with AMO are much larger than most other teleconnection patterns (Tables S2–S9). The clearest pattern of significant correlations with AMO was primarily on the NH extratropical contours, where a potential poleward change in the position of TTD contour of 0.3–2.0° may have resulted. This is equivalent to an average trend of 0.1–0.7° decade^{-1}, possibly a substantial fraction of the observed values.

Since 1989, significant negative trends in the AO and the NAO are also noted in Table 4. However, as noted earlier the correlation results with the TTD contours were unclear, and no consistent impact was readily identified. While there is no impact of these modes of climate variability on tropical expansion reported here, this should be further investigated using alternate approaches.

5. Summary and Discussion

In this study, the IGRA global radiosonde data set is used to examine the characteristics of tropical expansion in six broad regions around the globe. The analysis, which relies solely on observational data, follows the methodology described by *Lucas et al.* [2012]. Southern Hemisphere results are drawn from LNT12, while this study presents those from the NH and builds the broader global picture. Tropical expansion is determined through an analysis of a time-latitude array of tropical tropopause days (TTD), the annual number of days where the tropopause is found above 14.5 km altitude. This array is contoured, and temporal changes in the contour positions are used as the measure of tropical expansion. The focus of the analysis is on the subtropics, loosely defined as the region between the 300 and 50 day TTD contours. One aim of this research is to compare regional and hemispheric characteristics of tropical expansion. A second

aim is to identify the influences of patterns of climate variability on the TTD contours at interannual and longer-term time scales using partial correlation/regression techniques. Figure 7 summarizes the key findings of this study.

There are notable differences in tropical expansion across the different regions of the globe. Since 1979, tropical expansion is largest over ANZ and ASIA and smallest over NA and AFR. Between hemispheres, expansion appears to be largest in the SH, although this difference is not statistically significant.

These results broadly agree with the SH regional variability described by *Choi et al.* [2014], where the greatest expansion in the subtropical ridge is observed in Australia and South America. They also show large differences in the expansion rate over the central Pacific in their reanalysis-based calculations compared to the observed values. Unfortunately, sufficient radiosonde data are not available in that region to provide a direct comparison with their results. In general, the comparison of observations and reanalysis highlights some of the potential issues regarding the use of reanalysis products, with particular regard to the makeup of the observing system at a given location. The results here and in LNT12 suggest that the reanalysis products perform better in regions where there is a large component of data from the terrestrial observing system, consistent with *Bengtsson et al.* [2004]. Over relatively data poor regions like ASIA and AFR, the trend estimates are further from observations and a latitudinal shift between TTD contours from observations and reanalyses is larger. More concerning, the ERA-I indicates a change in this shift in both the NH and SH around 2002 that is suggestive of an inhomogeneity in that product. A hypothesis for this inhomogeneity, discussed in LNT12, is that it is the result of changes to the satellite observing system around this time. This likely explains the significant differences in trends between the ERA-I and the other reanalyses and observations (Table 3).

The comparison of the regional results presented here with those derived by *Chen et al.* [2014b] is poor. Overall, that study indicated stronger rates of expansion that was observed in different locations. These differences are broadly consistent with other satellite-based studies of tropical expansion, which generally show different results from studies using other metrics. Following *Lucas et al.* [2014], a plausible explanation for these differences is the choice to use OLR as a metric, which if uncorrected contain equatorial crossing time biases that introduce inhomogeneities into the record and inflate the trend estimates, particularly over land. Objective removal of these biases eliminates the tropical expansion trends, a result that is more physically consistent with expectations from modeling studies examining OLR in future climates [e.g., *Huang and Ramaswamy*, 2009]. The regional expansion in *Chen et al.* [2014b] follows this pattern; land sectors of the NH show strong expansion, while the primarily oceanic sectors in the SH show less. Hence, we hypothesize that their results are an artefact of the data set and not representative of the true regional variability in tropical expansion.

Partial correlation and regression analyses are used to link TTD contour positions to indices describing prominent modes of climate variability, suggesting that changes in these modes modulate the position of the tropical edge. The pattern with the most widespread effect is ENSO, identified both at the broadest spatiotemporal scales and in most regions and seasons. Generally, ENSO tends to expand the tropics during La Niña and contract them during El Niño, with the strongest effect on the extratropical TTD contours during JJA and SON. An opposite response in noted on the NA300 contour, particularly during DJF. With the other indices, significant correlations are mostly identified in individual regions and/or in particular seasons. Highly significant correlations are noted between the PDO and the contours in ASIA (and to a lesser extent EUR) during JJA and SON, on the ANZ contours with SAM during MAM, and with the AMO and the NH50 contour during MAM, with a regional focus on NA and EUR. Figure 7 indicates significant relationships with other indices as well.

The relationships noted above are focused on the interannual variability and represent short-term variations in position and not a contribution to the tropical expansion trend as such. However, several modes of climate variability show a persistent temporal change (Table 4), either through a decadal change in phase of an oscillation or an externally forced long-term trend. In these cases, an impact on tropical expansion can be identified. Since 1979, the change in PDO phase is responsible for up to 50% of the observed expansion trend, predominantly over ASIA. Previous studies [*Grassi et al.*, 2012; *Allen et al.*, 2014] have identified the PDO as a possible factor in NH tropical expansion. Outside of ASIA, a smaller portion of the trends may be driven by ENSO. In the SH, the long-term trend in SAM may contribute up to 20–30% of the expansion trend, mostly in the ANZ

region. The ASIA and ANZ regions generally have the largest regional expansion trends and also show the strongest long-term effects from the modes of climate variability. Removing these effects of climate variability makes the observed tropical expansion more globally uniform and brings the observed values more into line with projected average rates from coupled models of 0.1–0.2° decade^{-1} [*Lucas et al.*, 2014; *Quan et al.*, 2014]. In regions that show little impact from the modes of climate variability (e.g., NA and AFR), observed expansion rates are near this value. In short, values of observed tropical expansion over the period of record (i.e., from 1979) appear to be inflated due to coincident changes in modes of climate variability. Further, these climate modes have regional signatures which make tropical expansion nonuniform around the globe, potentially acting to modulate the observed impacts, for better or worse.

The physical mechanisms by which the modes of climate variability affect tropical expansion are unclear at present. Those examined here that are more interannual in nature (e.g., ENSO and SAM) are possibly driven more by a dynamical mechanism. As noted in the Introduction, these modes are often associated with shifts in the locations of the storm tracks and the associated eddy driven jet stream. These shifts have been related to interannual changes in the character of extratropical baroclinic waves and the "critical latitudes" at which they break [e.g., *Chen and Held*, 2007; *Chen et al.*, 2008]. This dynamical mechanism is also clearly linked to interannual variability of the SH summer Hadley Circulation [e.g., *Ceppi and Hartmann*, 2013]. In the NH, signals of this mechanism are less clear, as the large continents and topographic stationary wave patterns play a more significant role in the circulation there. This may account for the larger regional variability in that hemisphere. Nonlinear responses to ENSO have been noted in the NH [e.g., *Hoerling et al.*, 1997]; this may be responsible for the atypical response of the TTD contours over NA.

For the longer decadal-scale patterns (i.e., PDO and AMO), the changes to the underlying SST patterns may be more significant than the dynamical response. *Staten et al.* [2012] and *Quan et al.* [2014] have linked changes in SST to tropical expansion. These decadal modes are characterized by changes in the meridional distribution of SST. Idealized simulations [e.g., *Allen et al.*, 2012b; *Tandon et al.*, 2013] have suggested that anomalous heating of the midlatitudes acts to create tropical expansion through alteration of the meridional temperature gradient. The loading patterns for the PDO and AMO suggest temperature changes in these sensitive regions that coincide with the observed trend. *Allen et al.* [2014] implied that SST-type mechanisms were behind NH expansion; the observed expansion was attributed to PDO-driven SST changes, with the PDO variability forced by long-term changes in anthropogenic aerosol forcing.

The ongoing fluctuations of the modes of climate variability provide a powerful test of their hypothesized linkage to tropical expansion. On long (e.g., century) time scales, the expansion rate should tend toward the value determined by long-term climate forcing, while in the shorter term (e.g., decadal), the rate of tropical expansion will be more variable, a combination of climate forcing and the state of the climate modes. For example, if (and when) the PDO transitions to its warm phase, a slowdown or even a reversal of the NH tropical expansion would be expected. Similarly, the apparent slowdown in SH expansion since at least the early 2000s [*Ao and Hajj*, 2013] could be the result of the cessation of year-on-year growth of the Antarctic ozone hole [e.g., *World Meteorological Organization*, 2014] and the associated change in SAM. Over the longer term, an interesting question is whether the SH tropics will contract as the ozone recovers, or will the expected SAM increase from GHG [e.g., *Arblaster et al.*, 2011] prevent this from happening?

Appendix A

The paper makes extensive use of acronyms, particularly in section 4 where the results and their implications are discussed. This can make the text difficult to follow if the reader is not familiar with these acronyms. To allow the reader to more easily follow the discussion, section A1 lists the meaning of some of the more frequently used acronyms for easy reference.

A1. List of Frequent Acronyms

AFR	African region
AMO	Atlantic Multidecadal Oscillation
ANZ	Australia-New Zealand region
AO	Arctic Oscillation

ASIA	Asian region
ENSO	El Nino Southern Oscillation
ET	Extratropical TTD contours, i.e., 50 and 100 day
EUR	European region
NAO	North Atlantic Oscillation
NH	Northern Hemisphere
NA	North American region
PDO	Pacific Decadal Oscillation
PNA	Pacific North-America pattern
SA	South American region
SAM	Southern Annular Mode
SH	Southern Hemisphere
TR	Tropical TTD contours, i.e., 200 and 300 day
TTD	Tropical tropopause days, defined as number of days with ZT>14.5 km

Acknowledgments
The raw IGRA radiosonde data are available from the National Climatic Data Center (http://www.ncdc.noaa.gov/data-access/weather-balloon/integrated-global-radiosonde-archive). Information on accessing the reanalysis products used is available from http://reanalyses.org/atmosphere/overview-current-reanalyses. Processed data are available upon request from the corresponding author (c.lucas@bom.gov.au). This work was undertaken as part of the Victorian Climate Initiative (http://cawcr.gov.au/projects/vicci/), launched by the Victorian Department of Environment and Primary Industries, the Bureau of Meteorology and CSIRO. Pandora Hope and Scott Power provided useful comments on the manuscript, as did three anonymous reviewers.

References

Allen, R. J., S. C. Sherwood, J. R. Norris, and C. S. Zender (2012a), Recent Northern Hemisphere tropical expansion primarily driven by black carbon and tropospheric ozone, *Nature*, *485*, 350–354, doi:10.1038/nature11097.

Allen, R. J., S. C. Sherwood, J. R. Norris, and C. S. Zender (2012b), The equilibrium response to idealized thermal forcings in a comprehensive GCM: Implications for recent tropical expansion, *Atmos. Chem. Phys.*, *12*, 4795–4816, doi:10.5194/acp-12-4795-2012.

Allen, R. J., J. R. Norris, and M. Kovilakim (2014), Influence of anthropogenic aerosols and the Pacific Decadal Oscillation on tropical belt width, *Nat. Geosci.*, doi:10.1038/ngeo2091.

Ao, C. O., and A. J. Hajj (2013), Monitoring the width of the tropical belt with GPS radio occultation measurements, *Geophys. Res. Lett.*, *40*, 6236–6241, doi:10.1002/2013GL058203.

Arblaster, J. M., G. A. Meehl, and D. J. Karoly (2011), Future climate change in the Southern Hemisphere: Competing effects of ozone and greenhouse gases, *Geophys. Res. Lett.*, *38*, L02701, doi:10.1029/2010GL045384.

Bengtsson, L., K. I. Hodges, and S. Hagemann (2004), Sensitivity of the ERA40 reanalysis to the observing systems: Determination of the global atmospheric circulation from reduced observations, *Tellus, Ser. A*, *56*, 456–471.

Birner, T. (2010), Recent widening of the tropical belt from global tropopause statistics: Sensitivities, *J. Geophys. Res.*, *115*, D23109, doi:10.1029/2010JD014664.

Ceppi, P., and D. L. Hartmann (2013), On the speed of the eddy-driven jet and the width of the Hadley cell in the Southern Hemisphere, *J. Clim.*, *26*, 3450–3465, doi:10.1175/JCLI-D-12-00414.1.

Chen, G., and I. M. Held (2007), Phase speed spectra and the recent poleward shift of Southern Hemisphere surface westerlies, *Geophys. Res. Lett.*, *34*, L21805, doi:10.1029/2007GL031200.

Chen, G., J. Lu, and D. M. W. Frierson (2008), Phase speed spectra and the latitude of surface westerlies: Interannual variability and global warming trend, *J. Clim.*, *21*, 5942–5959, doi:10.1175/2008JCLI2306.1.

Chen, S., B. Yu, and W. Chen (2014a), An analysis on the physical process of the influence of AO on ENSO, *Clim. Dyn.*, *42*, 973–989, doi:10.1007/s00382-012-1654-z.

Chen, S., K. Wei, W. Chen, and L. Song (2014b), Regional changes in the annual mean Hadley circulation in recent decades, *J. Geophys. Res. Atmos.*, *119*, 7815–7832, doi:10.1002/2014JD021540.

Choi, J., S.-W. Son, J. Lu, and S.-K. Min (2014), Further observational evidence of Hadley cell widening in the Southern Hemisphere, *Geophys. Res. Lett.*, *41*, 2590–2597, doi:10.1002/2014GL059426.

Davis, S. M., and K. H. Rosenlof (2012), A multi-diagnostic intercomparison of tropical width time series using reanalyses and satellite observations, *J. Clim.*, *25*, 1061–1078, doi:10.1175/JCLI-D-11-00127.1.

Dee, D. P., et al. (2011), The ERA-Interim reanalysis: Configuration and performance of the data assimilation system, *Q. J. R. Meteorol. Soc.*, *137*, 553–597, doi:10.1002/qj.828.

Durre, I., R. S. Vose, and D. B. Wuertz (2006), Overview of the Integrated Global Radiosonde Archive, *J. Clim.*, *19*, 53–68, doi:10.1175/JCLI3594.1.

Enfield, D. B., A. M. Mestas-Nunez, and P. J. Trimble (2001), The Atlantic Multidecadal Oscillation and its relationship to rainfall and river flows in the continental U.S, *Geophys. Res. Lett.*, *28*, 2077–2080, doi:10.1029/2000GL012745.

Folland, C. K., J. Knight, H. W. Linderholm, D. Fereday, S. Ineson, and J. W. Hurrell (2009), The Summer North Atlantic Oscillation: Past, present, and future, *J. Clim.*, *22*, 1082–1103, doi:10.1175/2008JCLI2459.1.

Free, M., and J. K. Angell (2002), Effect of volcanos on the vertical temperature profile in radiosonde data, *J. Geophys. Res.*, *107*(D10), 4101, doi:10.1029/2001JD001128.

Free, M., and J. R. Lanzante (2009), Effect of volcanic eruptions on the vertical temperature profiles in radiosonde data and climate models, *J. Clim.*, *22*, 2925–2939, doi:10.1175/2008JCLI2562.1.

Free, M., J. K. Angell, I. Durre, J. Lazante, T. C. Peterson, and D. J. Seidel (2004), Using first differences to reduce inhomogeneity in radiosonde temperature datasets, *J. Clim.*, *17*, 4171–4179, doi:10.1175/JCLI3198.1.

Grassi, B., G. Redaelli, P. O. Canziani, and G. Visconti (2012), Effects of the PDO Phase on the tropical belt width, *J. Clim.*, *25*, 3282–3290, doi:10.1175/JCLI-D-11-00244.1.

Grise, K. M., S.-W. Son, and J. R. Gyakum (2013), Intraseasonal and interannual variability in North American storm tracks and its relationship to equatorial Pacific variability, *Mon. Weather Rev.*, *141*, 3610–3625, doi:10.1175/MWR-D-12-00322.1.

Hendon, H. H., E. Lim, and H. Nguyen (2014), Seasonal variations of subtropical precipitation associated with the Southern Annular Mode, *J. Clim.*, *27*, 3446–3460, doi:10.1175/JCLI-D-13-00550.1.

Hoerling, M. P., A. Kumar, and M. Zhong (1997), El Niño, La Niña, and the nonlinearity of their teleconnections, *J. Clim.*, *10*, 1769–1786, doi:10.1175/1520-0442(1997)010<1769:ENOLNA>2.0.CO;2.

Huang, Y., and V. Ramaswamy (2009), Evolution and trend of the outgoing longwave radiation spectrum, *J. Clim.*, *22*, 4637–4651, doi:10.1175/2009JCLI2874.1.
Hurrell, J. W., Y. Kushnir, G. Ottersen, and M. Visbeck (2003), An overview of the North Atlantic Oscillation, in *North Atlantic Oscillation: Climatic Significance and Environmental Impact*, *Geophys. Monogr. Ser.*, vol. 134, pp. 1–35, AGU, Washington, D. C.
Johanson, C. M., and Q. Fu (2009), Hadley cell widening: Model simulations versus observations, *J. Clim.*, *22*, 2713–2725, doi:10.1175/2008JCLI2620.1.
Kalnay, E., et al. (1996), The NMC/NCAR 40-Year Reanalysis Project, *Bull. Am. Meteorol. Soc.*, *77*, 437–471, doi:10.1175/1520-0477(1996)077<0437:TNYRP>2.0.CO;2.
Kanamitsu, M., W. Ebisuzakai, J. Woollen, S.-K. Yang, J. J. Hnilo, M. Fiorino, and G. L. Potter (2002), NCEP-DOE AMIP-II reanalysis (R-2), *Bull. Am. Meteorol. Soc.*, *83*, 1631–1643, doi:10.1175/BAMS-83-11-1631.
Knight, J. R., C. K. Folland, and A. A. Scaife (2006), Climate impacts of the Atlantic Multidecadal Oscillation, *Geophys. Res. Lett.*, *33*, L17706, doi:10.1029/2006GL026242.
Lanzante, J. R. (2005), A cautionary note on the use of error bars, *J. Clim.*, *18*, 3699–3703, doi:10.1175/JCLI3499.1.
Leathers, D. J., B. Yarnal, and M. A. Palecki (1991), The Pacific/North American teleconnection pattern and United States climate. Part I: Regional temperature and precipitation associations, *J. Clim.*, *4*, 517–528, doi:10.1175/1520-0442(1991)004<0517:TPATPA>2.0.CO;2.
Lucas, C., H. Nguyen, and B. Timbal (2012), An observational analysis of Southern Hemisphere tropical expansion, *J. Geophys. Res.*, *117*, D17112, doi:10.1029/2011LJD017033.
Lucas, C., B. Timbal, and H. Nguyen (2014), The expanding tropics: A critical assessment of the observational and modelling studies, *WIREs Clim. Change*, doi:10.1002/wcc.251.
Mantua, N. J., and S. R. Hare (2002), The Pacific decadal oscillation, *J. Oceanogr.*, *58*, 35–44, doi:10.1023/A:1015820616384.
Marshall, G. J. (2003), Trends in the Southern Annular Mode from observations and reanalyses, *J. Clim.*, *16*, 4134–4143, doi:10.1175/1520-0442(2003)016%3C4134:TITSAM%3E2.0.CO;2.
Min, S.-K., and S.-W. Son (2013), Multimodel attribution of the Southern Hemisphere Hadley cell widening: Major role of ozone depletion, *J. Geophys. Res. Atmos.*, *118*, 3007–3015, doi:10.1002/jgrd.50232.
Moore, R. W., O. Martius, and T. Spengler (2010), The modulation of the subtropical and extratropical atmosphere in the Pacific basin in response to the Madden-Julian Oscillation, *Mon. Weather Rev.*, *138*, 2761–2779, doi:10.1175/2010MWR3194.1.
Nguyen, H., A. Evans, C. Lucas, I. Smith, and B. Timbal (2013), The Hadley circulation in reanalyses: Climatology, variability and expansion, *J. Clim.*, *26*, 3357–3376, doi:10.1175/JCLI-D-12-00224.
Oort, A. H., and J. J. Yienger (1996), Observed interannual variability in the Hadley circulation and its connection to ENSO, *J. Clim.*, *9*, 2751–2767, doi:10.1175/1520-0442(1996)009<2751:OIVITH>2.0.CO;2.
Panofsky, H. A., and G. W. Brier (1968), *Some Applications of Statistics to Meteorology*, 224 pp., The Pennsylvania State Univ, Univ. Park, Pa.
Peterson, T. C., and D. R. Easterling (1994), Creation of homogeneous composite climatological reference series, *Int. J. Climatol.*, *14*, 671–679, doi:10.1002/joc.3370140606.
Peterson, T. C., T. R. Karl, P. F. Jamason, R. Knight, and D. R. Easterling (1998), First difference method: Maximizing station density for the calculation of long-term global temperature change, *J. Geophys. Res.*, *103*, 25,967–25,974, doi:10.1029/98JD01168.
Polvani, L. M., D. W. Waugh, G. J. P. Correa, and S.-W. Son (2011), Stratospheric ozone depletion: The main driver of twentieth-century atmospheric circulation changes in the Southern Hemisphere, *J. Clim.*, *24*, 795–812, doi:10.1175/2010JCLI3772.1.
Quan, X.-W., M. P. Hoerling, J. Perlwitz, H. F. Diaz, and T. Xu (2014), How fast are the tropics expanding?, *J. Clim.*, *27*, 1999–2013, doi:10.1175/JCLI-D-13-00287.1.
Reichler, T., M. Dameris, and R. Sausen (2003), Determining the tropopause height from gridded data, *Geophys. Res. Lett.*, *30*(20), 2042, doi:10.1029/2003GL018240.
Santer, B. D., et al. (2003), Contributions of anthropogenic and natural forcing to recent tropopause height changes, *Science*, *301*, 479–483, doi:10.1126/science.1084123.
Schlesinger, M. E., and N. Ramankutty (1994), An oscillation in the global climate system of period 65–70 years, *Nature*, *367*, 723–726, doi:10.1038/367723a0.
Seager, R., N. Niak, and G. A. Vecchi (2010), Thermodynamic and dynamic mechanisms for large-scale changes in the hydrological cycle in response to global warming, *J. Clim.*, *23*, 4651–4668, doi:10.1175/2010JCLI13655.1.
Seidel, D. J., and W. J. Randel (2007), Recent widening of the tropical belt: Evidence from tropopause observations, *J. Geophys. Res.*, *112*, D20113, doi:10.1029/2007JD008861.
Son, S.-W., N. F. Tandon, L. M. Polvani, and D. W. Waugh (2009), Ozone hole and southern hemisphere climate change, *Geophys. Res. Lett.*, *36*, L15705, doi:10.1029/2009GL038671.
Son, S.-W., et al. (2010), Impact of stratospheric ozone on Southern Hemisphere circulation change: A multimodel assessment, *J. Geophys. Res.*, *115*, D00M07, doi:10.1029/2010JD014271.
Staten, P. W., J. J. Rutz, T. Reichler, and J. Lu (2012), Breaking down the tropospheric circulation response by forcing, *Clim. Dyn.*, *39*, 2361–2375, doi:10.1007/s00382-011-1267-y.
Tandon, N. F., E. P. Gerber, A. H. Sobel, and L. M. Polvani (2013), Understanding Hadley cell expansion vs. contraction: Insights from simplified models and implications for recent observations, *J. Clim.*, *26*, 4304–4321, doi:10.1175/JCLI-D-12-00598.1.
Thompson, D. W. J., and J. M. Wallace (1998), The Arctic oscillation signature in the wintertime geopotential height and temperature fields, *Geophys. Res. Lett.*, *25*, 1297–1300, doi:10.1029/98GL00950.
Uppala, S. M., et al. (2005), The ERA-40 reanalysis, *Q. J. R. Meteorol. Soc.*, *131*, 2961–3012, doi:10.1256/qj.04.176.
Verdon, D. C., and S. W. Franks (2006), Long-term behaviour of ENSO: Interactions with the PDO over the past 400 years inferred from paleoclimate records, *Geophys. Res. Lett.*, *33*, L06712, doi:10.1029/2005GL025052.
Wolter, K., and M. S. Timlin (1998), Measuring the strength of ENSO events: How does 1997/98 rank?, *Weather*, *53*, 315–324.
World Meteorological Organization (2014), Assessment for Decision-Makers: Scientific Assessment of Ozone Depletion: 2014, World Meteorological Organization, Global Ozone Research and Monitoring Project—Rep., 56, Geneva, Switzerland.
Wunsch, C. (1999), The interpretation of short climate records, with comments on the North Atlantic and Southern Oscillations, *Bull. Am. Meteorol. Soc.*, *80*, 245–255, doi:10.1175/1520-0477(1999)080%3C0245:TIOSCR%3E2.0.CO;2.
Zhang, C. (2005), Madden-Julian Oscillation, *Rev. Geophys.*, *43*, RG2003, doi:10.1029/2004RG000158.